Journal of Statistical Mechanics:
Theory and Experiment



PAPER

# Variability of entropy force and its coupling with electrostatic and steric hindrance interactions

Journal of Statistical Mechanics: Theory and Experiment
An IOP and SISSA journal

PAPER: Classical statistical mechanics, equilibrium and non-equilibrium

# Variability of entropy force and its coupling with electrostatic and steric hindrance interactions

**S Zhou**

School of Physics, Central South University, Changsha, Hunan 410083, People's Republic of China
E-mail: chixiayzsq@163.com

Received 22 November 2023
Accepted for publication 13 March 2024
Published 17 April 2024

Online at stacks.iop.org/JSTAT/2024/043202
https://doi.org/10.1088/1742-5468/ad363e

**Abstract.** We investigated the effective interaction potential (EIP) between charged surfaces in solvent comprised of dipole dimer molecules added with a certain amount of ionic liquid. Using classical density functional theory, the EIP is calculated and decoupled into entropic and energy terms. Unlike the traditional Asakura–Oosawa (AO) depletion model, the present entropic term can be positive or negative, depending on the entropy change associated with solvent molecule migration from bulk into slit pore. This is determined by pore congestion and disruption of the bulk dipole network. The energy term is determined by the free energy associated with hard-core repulsion and electrostatic interactions between surface charges, ion charges, and polarized charges carried by the dipole dimer molecules. The calculations in this article clearly demonstrate the variability of the entropy term, which contrasts sharply with the traditional AO depletion model, and the corrective effects of electrostatic and spatial hindrance interactions on the total EIP; we revealed several non-monotonic behaviors of the EIP and its entropic and energy terms concerning solvent bulk concentration and solvent molecule dipole moment; additionally, we demonstrated the promoting effect of dipolar solvent on the emergence of like-charge attraction, even in 1:1 electrolyte solutions. The microscopic origin of the aforementioned phenomena was analyzed to be due to the non-monotonic change of dipolar solvent adsorption with dipole moment under conditions of low solution dielectric constant. The present findings offer novel approaches and molecular-level guidance for regulating the EIP. This insight has implications for understanding fundamental processes in various fields, including biomolecule-ligand binding, activation energy

barriers, ion tunneling transport, as well as the formation of hierarchical structures, such as mesophases, micro-, and nanostructures, and beyond.

**Keywords:** depletion interaction, solvent polarity, ionic liquid, entropic driven potential

Supplementary material for this article is available online

## Contents

1. Introduction ..... 2
2. Model and method ..... 4
3. Discussion ..... 8
4. Summary ..... 26
References ..... 27

## 1. Introduction

The potential of mean force, or effective interaction potential (EIP), between particles (where the term 'particle' encompasses molecules, colloidal particles, and clusters) plays a crucial role in various contexts, such as collision rates [1, 2], dispersion stability [3–5], ion-ligand association [6, 7], particle assembly [8], enrichment and fractionation during hydrothermal transport process [9, 10]. Although the EIP acquires distinct names in different situations, the underlying phenomena share common features. For instance, when a mixture of neutral, sterically stabilized colloids and non-adsorbing polymers is formed, the presence of neutral polymers can induce diverse phenomena, including fluid–fluid phase separation and the formation of gels or attractive glasses. This occurs due to the induced inter-colloid effective interaction—known as the entropic driven depletion potential—arising from the excluded volume repulsion between colloids and polymers [11–14]. Similarly, when hydrophobic particles (with hydrophobicity denoting an aversion or lack of affinity for water) are immersed in an aqueous environment, the water-mediated EIP between the hydrophobic particles is referred to as the hydrophobic interaction potential [15–17]. Hydrophobic interactions play a significant role in numerous processes occurring in aqueous solutions. These interactions are particularly important in complexation, surfactant aggregation, coagulation, molecular recognition, the development of waterproof coatings, and the formation and stabilization of proteins, biological membranes, and micelles [18–22]. The EIP between charged colloids in ion fluids is referred to as the effective electrostatic potential (EEP) [23–30], which arises from the interplay of electrical forces in the presence of other ions in the surrounding solution and is influenced by several factors, including surface charge, double layer, ionic



J. Stat. Mech. (2024) 043202

strength, Debye length (which characterizes the screening of electrostatic interactions in a solution), and steric effects. Understanding and controlling the EEP between colloids is essential for various applications, such as stabilizing or destabilizing colloidal dispersions, emulsions, and suspensions [31, 32], designing effective drug delivery systems [33, 34], and creating products with specific adhesion and durability properties [35]. The Casimir force is also a type of effective interaction that manifests as an attractive force between two uncharged, closely spaced objects in a vacuum or a dielectric medium [36, 37]. According to Lifshitz theory [38], this force results from fluctuations in the electromagnetic field, which arise due to the inherent uncertainty principle in quantum mechanics. At the nanoscale, the Casimir force can substantially influence the behavior of micro- and nanoscale devices, contributing to the development of nanoelectromechanical systems [39]. Furthermore, the Casimir force is among the numerous factors that affect the stability and behavior of colloidal systems. Depending on the specific conditions and the interplay of other forces, it can either promote aggregation (when attractive) or hinder it (when repulsive) [37, 40–42].

Among the four EIPs mentioned above, the depletion potential is primarily driven by entropic contributions, while the hydrophobic interaction is determined by the repulsion and attraction between neutral particles [43], system temperature and salt concentration [44], and the interplay with solute size and shape [45]. The effective electrostatic interaction is mainly controlled by the electrostatic force between ions and charged surfaces. The Casimir force relies on several factors, such as the objects' geometry, the materials they are made of, medium properties, and ion screening. Under specific conditions, the Casimir force can be altered from attractive to repulsive [46].

However, in a broader sense, multiple forces between particles frequently coexist, making it difficult to neatly categorize EIPs into distinct types. Instead, each category of EIP has its historical reasons and unique characteristics. These complexities highlight the need for a comprehensive understanding of the various forces' interplay and their combined effects on particle behaviors in assorted systems.

The rich diversity and complexity of intermolecular forces, surface properties, and suspension compositions bestow upon EIPs a wide range of intriguing behaviors and characteristics. These unique attributes open up new avenues for practical applications in various fields, prompting further exploration into the underlying principles and potential uses of EIPs to help harness their benefits and contribute to advancements in scientific research and technology [47–49].

A polar molecule is composed of atoms or atomic groups with varying electronegativity. This difference in electronegativity causes a charge separation within the polar molecule, creating a positively polarized end and a negatively polarized end. One of the most well-known examples of polar molecules is water ($H_2O$). In a water molecule, the oxygen atom is more electronegative than the hydrogen atoms, leading to an unequal sharing of electrons. Consequently, the oxygen atom acquires a partially negative charge, while the hydrogen atoms exhibit a partially positive charge. Other common polar molecules include ethanol, acetone, acetonitrile, and methanol. The unique properties of polar molecules allow for a wide range of applications in various fields. These applications encompass chemical reactions, solubility, environmental remediation, medicine and pharmaceuticals, membrane permeability, cell signaling, and the maintenance of cellular

J. Stat. Mech. (2024) 043202

environments. The versatility of polar molecules stems from their distinct characteristics and underpins their significance in numerous scientific and industrial applications.

Ionic liquids (ILs) constitute a class of organic salts that exhibit a liquid state at or near room temperatures. Composed of positively charged ions (cations) and negatively charged ions (anions), ILs possess a unique combination of properties, such as tunability, low volatility, and high thermal stability. These properties make them suitable for various applications, including green solvents, electrolytes, catalysts, supercritical fluids, nanotechnology, chemical sensors, and energy storage. ILs can also potentially affect cell functions through several mechanisms, such as cell membrane interactions, cell viability and cytotoxicity, cell signaling, and gene expression. The impact of ILs on cell function is highly context-dependent and can vary based on the specific chemical composition of the IL used, its concentration, and the type of cells involved. This inherent contextual variability necessitates a thorough understanding of the interactions between ILs and biological systems to safely and effectively harness their potential in various applications.

The objective of the present work is to examine the EEP between two charged surfaces in a medium composed of solvents with varying polarities and ILs, as well as to investigate the morphological characteristics and variations of the EEP curves concerning system parameters. The focus lies in exploring the possible variability of entropy changes and the consequent entropy term in the EEP as functions of solvent polarities and solvent bulk concentrations. Understanding and controlling the EEP of charged surfaces in such environments is crucial for a variety of applications, including the design of colloidal materials, the development of new sensors, and the manipulation of nanostructures.

This paper is structured as follows. In section 2, we provide a brief description of the model defining the system, which consists of a neutral or polar solvent, IL, and two charged surfaces, along with the classical density functional theory (cDFT) employed to calculate the EEP. In section 3, we present theoretical results for the EEP and its two decoupled terms: entropy and energy terms. Additionally, we conduct a thorough theoretical analysis of the variation patterns of the potential energy curve, its decoupled terms, and the corresponding molecular mechanisms. Lastly, in section 4, we summarize the main findings and conclusions of this study.

## 2. Model and method

The current system is composed of two charged flat plates oriented face-to-face, solvent molecules, and ILs with specific bulk mole concentrations denoted as $c_s$ and $c_{il}$, respectively. Surface charges are typically generated via chemical functionalization or ionization of surface groups. We assume that these surface charges are uniformly distributed across the surface, characterized by a surface charge density $\sigma$. In this model, positive monovalent cations and negative monovalent anions of the IL are represented as centrally charged hard spheres. Since ILs typically consist of large organic cations and small inorganic anions, their respective hard sphere diameters are set at 4 Å and 2.4 Å. The polar solvent molecule is modeled as a dimer, composed of two hard spheres with equal diameters of 1.92 Å each. One end of the dimer is positively polarized, while the other



J. Stat. Mech. (2024) 043202

end is negatively polarized. Each end possesses a polarization charge of equal intensity, denoted as $\delta e$, where $e$ represents the elementary charge strength. The presence of separated positive and negative charges within a molecule leads to the formation of an electric dipole. Its electrical characteristics are commonly represented by the electric dipole moment, denoted as $\mu$. The electric dipole moment can be calculated using the following formula:

$$\mu = \delta e d. \tag{1}$$

In this formula, $d$ represents the separation distance between the positively and negatively polarized charges, $d = 1.92$ Å within the current context. The dipole moment is extensively employed in physics and chemistry to elucidate various phenomena, encompassing intermolecular interactions and solute-solvent interactions in solutions.

In our model, we disregard the van der Waals interactions between particles, as they arise from electron density fluctuations and are generally weak and short-ranged, particularly when compared to electrostatic interactions. This is especially true in certain regions of the current system, which belong to a strongly correlated electrostatic regime. The details of the cDFT method employed can be found in the literature [50] and are not reiterated here; however, the principal equations involved are provided below. Given that the system under investigation operates in high concentration and strong confinement regimes, packing effects become overwhelmingly significant. It is crucial to address how finite-size effects are accounted for. In addition, because the system is in a strong coupling regime with a relatively low relative dielectric constant of 5, electrostatic correlations play a vital role. Therefore, we offer a discussion on the approximations employed beyond the mean-field level to account for such strong correlations.

Internal excess Helmholtz free energy $F_{\mathrm{ex}}[\{\rho_i\}]$ can be decomposed into sum of four terms:

$$F_{\mathrm{ex}}[\{\rho_i\}] = F_{rep}[\{\rho_i\}] + F_{ele}[\{\rho_i\}] + F_{coup}[\{\rho_i\}] + F_{assoc}[\{\rho_i\}], \tag{2}$$

where $F_{rep}[\{\rho_i\}]$ describes the free energy caused by hard repulsion between four types of particle, i.e. cation, anion, positive and negative ends; $F_{ele}[\{\rho_i\}]$ represents a long-range mean field electrostatic interaction free energy; $F_{coup}[\{\rho_i\}]$ deals with a free energy coming from short-range coupling effect between hard repulsion and electrostatic interaction. $F_{assoc}[\{\rho_i\}]$ associated with the formation of a molecule through the bonding of positive and negative ends is constructed using a modified interfacial statistical associating fluid theory; the applicability of this theory to a variety of inhomogeneous complex fluids is demonstrated through Monte Carlo simulations [51].

We will employ the fundamental measure theory (FMT) to tackle the $F_{rep}[\{\rho_i\}]$. Initially developed by Rosenfeld [52], the FMT is a highly-regarded and accurate model within the field of cDFT for hard spheres. It originated from the exact results of Percus and coauthors [53, 54] for one-dimensional systems along with an approximate description of hard-sphere statistical mechanics known as Scaled Particle Theory [55]. Since its introduction, numerous modifications and improvements have been proposed [56], particularly the so-called dimensional crossover approach [57]. This method aims to work out the details for $F_{rep}[\{\rho_i\}]$ by requiring the theory in three dimensions to reproduce the exact lower-dimensional functionals when suitably restricted. This inspired the



J. Stat. Mech. (2024) 043202

sophisticated modern 'White Bear' functionals [58], which provide an excellent description of inhomogeneous hard-sphere systems, including the freezing transition, and were, for some time, considered the best available model. In this paper, we utilize the 'White Bear' functionals [58] that account for the correct 'dimensional crossover' behavior and are compatible with the Mansoori–Carnahan–Starling–Leland equation of state [59].

Both terms, $F_{ele}[\{\rho_i\}]$ and $F_{coup}[\{\rho_i\}]$, originate from the second-order functional perturbation expansion of the Helmholtz free energy of an inhomogeneous fluid around that of a coexisting homogeneous fluid. The expansion coefficients are based on the bulk direct correlation functions obtained from the Ornstein–Zernike integral equation with the mean spherical approximation (MSA) closure [60, 61]. The part of MSA's second-order direct correlation functions greater than the hard-sphere diameter is precisely the negative electrostatic interaction potential between ions divided by the average thermal energy $k_BT$. As a result, its mathematical form is akin to the mean field approximation; therefore, we refer to $F_{ele}[\{\rho_i\}]$ as 'the treatment of long-range electrostatic interactions using the mean field approximation'. The expansion coefficients for $F_{coup}[\{\rho_i\}]$ are the portions of MSA's second-order direct correlation functions that are less than the hard-sphere diameter, subtracted by the Percus–Yevick approximation's second-order direct correlation functions [62] for the corresponding multicomponent hard-sphere mixture (with all particle charges removed). When all particles are neutral and uncharged, this difference is zero. Consequently, this expansion coefficient originates from the coupling of electrostatic and hard-sphere interactions, hence $F_{coup}[\{\rho_i\}]$ can be reasonably referred to as the correlation effect between hard-sphere and electrostatic interactions.

The reliability of the second-order $F_{coup}[\{\rho_i\}]$ term combined with the FMF for strongly correlated systems has been established through simulation calculations. In electrostatic systems, 'strong correlation' typically arises from the interplay of high density, high ionic charge, and low relative permittivity. The first factor leads to a strong spatial steric effect, which drives the system's free energy into a region more sensitive to particle density distribution. In contrast, the latter two factors intensify electrostatic interactions between charges. The combined influence of these three factors enhances the correlation effect between hard-sphere and electrostatic interactions. As a result, strongly correlated systems present a rigorous test for perturbation expansion. Zhou and Lamperski [63] demonstrated that the combination of the second-order $F_{coup}[\{\rho_i\}]$ term and FMF is reliable for investigating the electrical capacitance properties of extreme nanoscale supercapacitors (where electrical capacitance signifies the derivative of electrode charge density concerning electrode potential). Meanwhile, [64, 65] showed that even for tetravalent counterions, the combination yields reliable density and potential distribution profiles.

A current concern is that even though the ions studied are only monovalent, the relative permittivity employed in our calculations is 5, which represents a significant reduction compared to the 78.5 used in the aforementioned [63–65]. This decrease in relative permittivity substantially increases the correlation strength of our computational model, raising concerns about the potential impact on the reliability of the combination of the second-order $F_{coup}[\{\rho_i\}]$ term and FMF.

Fortunately, the relative permittivity of 5 is only a residual value accounting for the potential polarization of particles in the actual system. In our model, we employ



J. Stat. Mech. (2024) 043202

a solvent with a specific dipole moment. Such a polar solvent possesses a dielectric constant, which measures its ability to attenuate electrostatic interactions. Since we explicitly consider solvent molecules in the calculations, there is no need to repeatedly account for this dielectric constant by assigning an associated dielectric constant corresponding to the dipolar solvent on top of the residual dielectric constant. Thus, after explicitly incorporating solvent molecules and adjusting the model with a residual permittivity of 5, the actual electrostatic strength is not as pronounced as it would be with a sole relative permittivity of 5.

The total free energy $F[\{\rho_i\}]$ is available by combining $F_{\text{ex}}[\{\rho_i\}]$ with an analytically available ideal gas free energy

$$F[\{\rho_i\}] = F_{\text{ex}}[\{\rho_i\}] + \sum_i \int \mathrm{d}\boldsymbol{r}\rho_i(\boldsymbol{r})\left[\ln\left(\rho_i(\boldsymbol{r})\lambda_i{}^2 - 1\right)\right], \tag{3}$$

where $\lambda_i$ is the thermal de Broglie wavelength of the $i$th component. The $F[\{\rho_i\}]$ is converted into a grand potential functional $\Omega[\{\rho_i\}]$ by a Legendre transform. The variational principle of the giant potential gives the Euler–Lagrange equation. By numerically solving the equation, one obtains the equilibrium density distribution and relevant equilibrium grand potential $\Omega[\{\rho_i\}]$ and excess grand potential $\Omega_{\text{ex}}[\{\rho_i\}]$.

The EEP is system free energy change when the two surfaces change their distance from each other, and can be calculated as follows:

$$u(h) = \Omega_{\text{ex}}(h, [\{\rho_i\}]) - \Omega_{\text{ex}}(h_{\max}, [\{\rho_i\}]) \tag{4}$$

where $h_{\max}$ is a sufficiently large plate spacing, its further increase will no longer alter the excessive grand potential.

According to the basic thermodynamic formula, entropic term $u_s$ of the EEP can be calculated as follows

$$u_s = -T\Delta S, \tag{5}$$

$$\Delta S = -\frac{\partial u}{\partial T}. \tag{6}$$

We use EEPs of 298.15 K and 318.15 K and numerical differentiation to obtain the temperature partial derivative needed for the entropy change $\Delta S$ for target temperature 308.15 K:

$$\Delta S = -\frac{u|_{T=318.15} - u|_{T=298.15}}{\Delta T}, \tag{7}$$

where, $\Delta T = 20\,\text{K}$. We found that using a shorter temperature interval, for example $\Delta T = 10$ yields the same results; but too small $\Delta T$ may cause artificial oscillation of $\Delta S$. The $\Delta S$ obtained in this way corresponds to a system temperature of 308.15 K.

Energy term $u_e$ of the EEP is calculated by disposing of the $u_s$ from the total EEP $u$:

$$u_e = u - u_s. \tag{8}$$



J. Stat. Mech. (2024) 043202

If not specifically stated, the system temperature considered is always 298.15 K. Only when decoupling of the EEP needs to be calculated, system temperature of 308.15 K is considered. About the relative dielectric constant $\varepsilon_r$, In practical systems, molecules (whether polar or non polar) will further polarize in electric field, weakening the electrical double layer electric field; this is equivalent to increasing the $\varepsilon_r-$value. Therefore, we adopt a residual relative dielectric constant of $\varepsilon_r = 5.0$ to reflect this realistic situation.

Thermal motion average energy $k_BT$ and $d = 4$Å are used as energy unit and length unit, respectively. The $u$, $u_s$ and $u_e$ are expressed as reduced energy per unit surface area $u^* = ud^2/k_BT$, $u_s{}^* = u_sd^2/k_BT$ and $u_e{}^* = u_ed^2/k_BT$, respectively. The plate separation $h$ is reduced as $h^* = h/d$.

## 3. Discussion

Figures 1 and 2 show the potential energy curves for different solvent polarities and solvent concentrations. The solvent polarities considered span from $p = 0.0$D to $p = 4.0$D. In order to have a vivid understanding of the $p-$values, we have listed the $p-$values of several solvents. For example, Propylene carbonate has a $p-$value of 4.9D; Sulfolane, 4.8D; $\gamma$-butyrolactone, 4.27D; Dimethylsulfoxide (DMSO), 3.96D; Acetonitrile, 3.91D; Acetone, 2.88D, and Tetrahydrofuran,1.75D.

It should be pointed out that we have not drawn the potential energy curve and its decoupled terms in the range of $h^*$ less than 1.01, because particles are difficult to enter such a narrow space and numerical procedure is difficult to converge.

In the upper and middle subgraphs of figure 1, the potential curves are depicted as increasing monotonically with plate separation for neutral or weakly polar solvents (e.g. $p = 0.15$D). This trend continues until the separation is approximately equal to the sum of the counter-ion diameter and the solvent molecule length. Beyond this point, the potential energy remains relatively stable. In situations with low solvent concentrations, the potential energy decreases monotonically and approaches zero. However, at higher solvent concentrations, the potential energy may exhibit weak oscillations as it tends towards zero. When the plate separation is approximately equal to either the counter-ion diameter or the solvent molecule length, the potential becomes negative.

However, as the solvent polarity increases, the potential curve morphology changes significantly, as illustrated in the bottom subgraph of figures 1 and 2. When the plate separation is close to the counter-ion diameter or solvent molecule length, the potential energy is positive. As the plate separation increases, the potential energy decreases until it reaches the sum of the counter-ion diameter and the solvent molecule length, where the potential energy attains a minimum value. Subsequently, the potential energy increases and reaches a maximum value; then, the potential energy curve exhibits weak oscillations towards zero as the plate separation continues to increase.

In figure S1, we present a comprehensive view of the potential energy curves over a wide range of dipole moments, spanning from zero to 4.0D for a specific parameter combination. To enhance clarity, in figure 3 we have included the curves of potential energy versus dipole moment, focusing on the range of plate separation from 1.01 to 1.8 times the counter-ion diameter. Additionally, we display the minimum and maximum



J. Stat. Mech. (2024) 043202

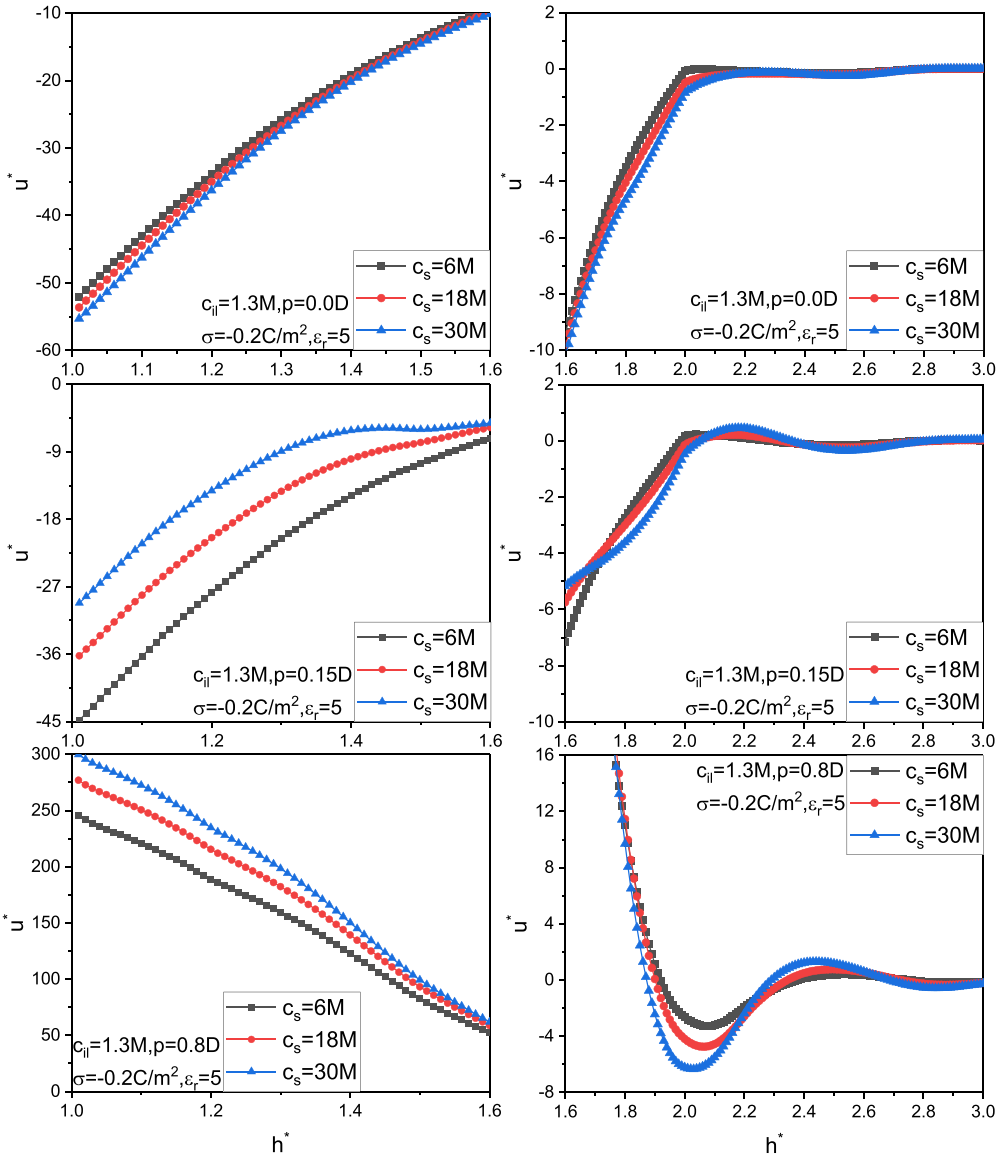


**Figure 1.** Variation of reduced effective interaction potential $u^*$ with solvent bulk mole concentration $c_s$ and solvent molecule dipole moment $p$. Top, middle, and bottom subgraphs correspond to $p = 0.0$D, 0.15D, and 0.8D, respectively. Other parameter values are indicated in the graphs and in the text.

potential energy values, along with their corresponding plate separation values, when the solvent polarity is not too low, allowing the potential energy curves to exhibit both maximum and minimum values.

From the upper subgraph of figure 1, we observe that when the dipole moment is zero, the near contact potentials (NCPs), primarily when the plate separation is less than or equal to 1.6, are significantly negative. Additionally, their strengths decrease with increasing plate separation, which is a typical attribute of the traditional depletion potential. Traditionally, the depletion potential behaviors are explained using a simple

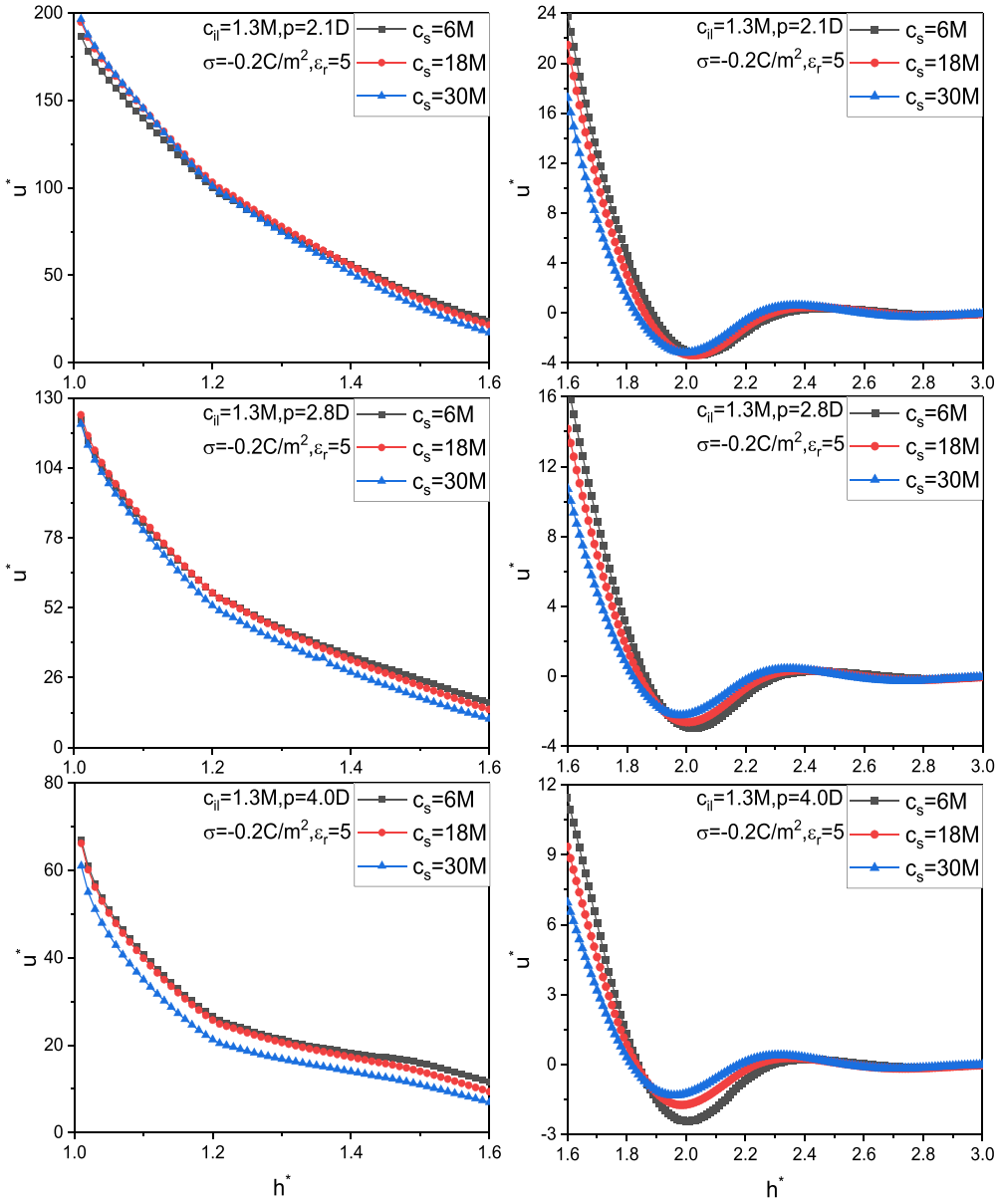


**Figure 2.** The same as in figure 1 except $p = 2.1\text{D}, 2.8\text{D},$ and 4.0D, respectively.

Asakura–Oosawa (AO) model, which considers the existence of a so-called depletion layer around each particle. Depletion agents, usually polymers, cannot penetrate this area. Overlapping depletion layers of two approaching colloids or surfaces suggest a larger free volume for polymers, leading to an increase in system entropy. The depletion potential's depth is mainly governed by polymer density, while its range correlates with the polymer radius of gyration.

The AO model portrays non-adsorbing polymer coils as fixed-size, effective spheres. However, this spherical polymer approximation overlooks the conformational diversity of the polymer depletant, which can considerably influence system entropy. Moreover,

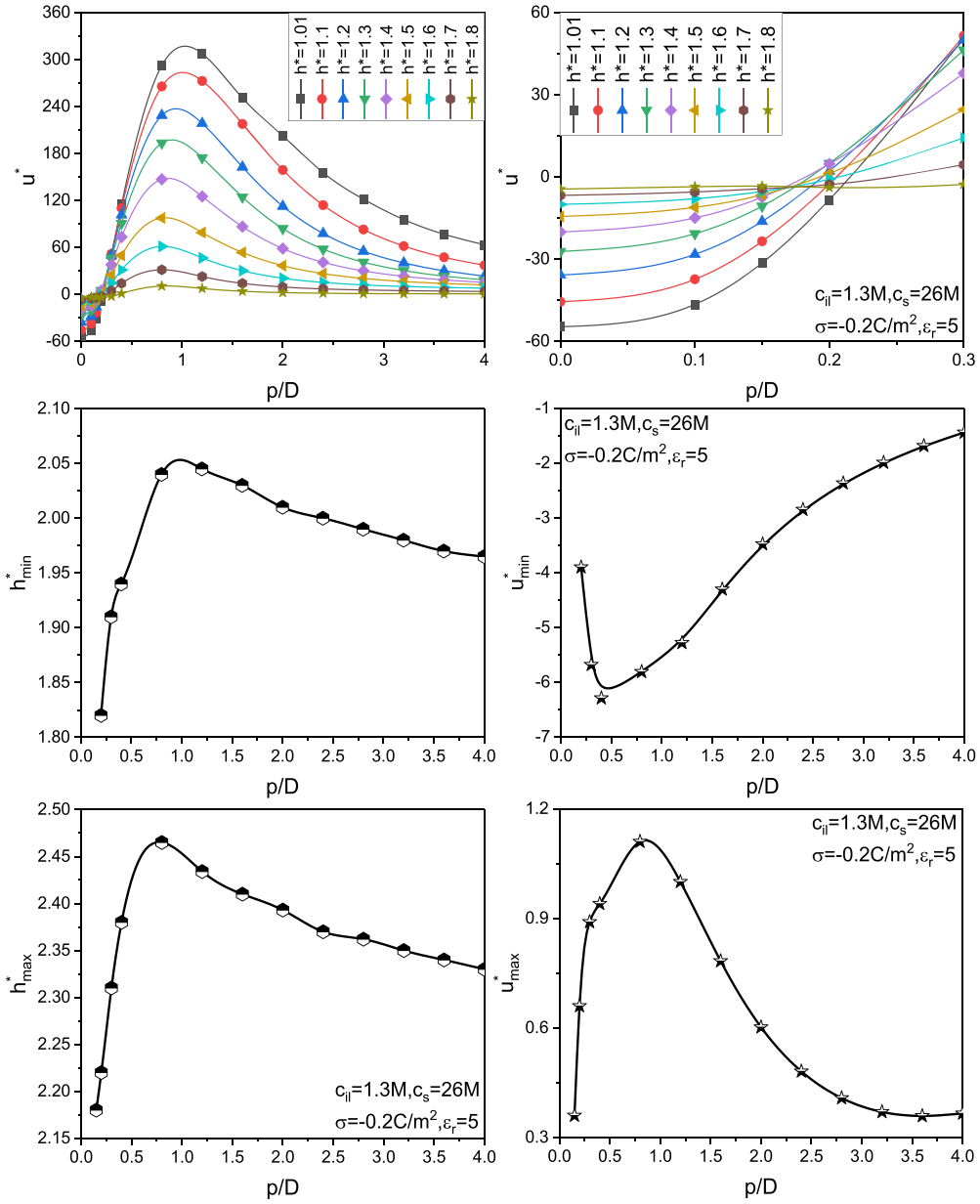


**Figure 3.** (Top subgraph) Variation of the near contact potential (NCP) with solvent molecule dipole moment $p$. The reduced surface separations considered are: $h^* = 1.01,\ 1.1,\ 1.2, 1.3,\ 1.4,\ 1.5,\ 1.6, 1.7,\ 1.8$. (Middle subgraph) Minimum of the potential energy curve and corresponding surface separation as a function of the solvent dipole moment $p$. (Bottom subgraph) Maximum of the potential energy curve and corresponding surface separation as a function of the solvent dipole moment $p$.

in the AO model, the interactions between effective spheres are neglected, considering only the interactions between effective spheres and colloidal particles. The current model incorporates both electrostatic and short-range repulsion interactions between surfaces,

ions, and sites of dimer depletant, as well as molecular non-sphericity, to account for real-world complexities. As we will learn from the following discussion, considering these real-world details causes the resulting EIP to exhibit both quantitative and qualitative deviations from the traditional depletion potential.

The curves presented in figures 1–3 illustrate non-monotonic variation trends of some key physical quantities related to the potential energy curves with respect to solvent dipole moment, bulk IL concentration, and reversible variation relationship between depth and location of like charge attraction (LCA) and ion concentration for different dipole moments. This implies the existence of an optimal combination of system parameters in practical applications. Understanding the occurrence mechanisms behind these 'anomalies' will theoretically assist in determining the optimal combination through experiments.

The six subgraphs in figures 1 and 2 display several different types of potential curves and their variations with the solvent dipole moment. The NCPs in both the top and middle subgraphs of figure 1 are attractive (first type NCP), while those in the bottom subgraph of figure 1 and all subgraphs of figure 2 are repulsive (second type NCP). The difference between the two first type NCPs lies in the fact that the attraction potential intensity of the former increases with the solvent bulk concentration $c_s$, while the latter decreases with the $c_s-$value. The second type NCP can be further subdivided into three subtypes, among which the bottom subgraph in figure 1 belongs to the first subtype—its NCP intensity increases with the $c_s-$value. The top subgraph of figure 2 pertains to the second subtype, in which the NCP intensity is not sensitive to the $c_s-$value, and the relationship between the NCP and the $c_s-$value appears to have small irregularities in different sections. Lastly, the middle and bottom subgraphs of figure 2 belong to the third subtype—here, their NCP intensities decrease with the $c_s-$value but are relatively unresponsive.

In figures 4–7, we illustrate the potential curves for four exemplary dipole moments along with their respective entropy and energy term curves. These four representative dipole moments, specifically 0.0D, 0.15D, 0.8D, and 4.0D, are featured in figures 1 and 2. Among these moments, for $p = 0.0$D and $p = 0.15$D, the associated potential curves belong to the first type; on the other hand, for $p = 0.8$D and 4.0D, the related potential curves pertain to the first and third subtypes of the second type. We did not fully replicate the potential curve calculations from figures 1 and 2. For the potential curves and their associated entropy and energy terms demonstrated in figures 4–7, the calculated temperature is 308.15 K, while the temperature considered in figures 1 and 2 is 298.15 K. This variation is due to the need to involve temperatures 10 K lower and 10 K higher than the target temperature when calculating the entropy increase in equation (6) using a numerical method; however, the cDFT is challenging to converge numerically at lower temperatures.

Let us first primarily analyze the behavior of non-NCPs as the system parameters change.

To make the following analysis more reasoned and grounded, rather than speculative, we need not only the EIP curve and its decoupled terms (entropy and energy terms) but also the distribution of particles within the pore. For this purpose, in figures 8–10, we plotted the solvent adsorption and the density distribution of various particles



J. Stat. Mech. (2024) 043202

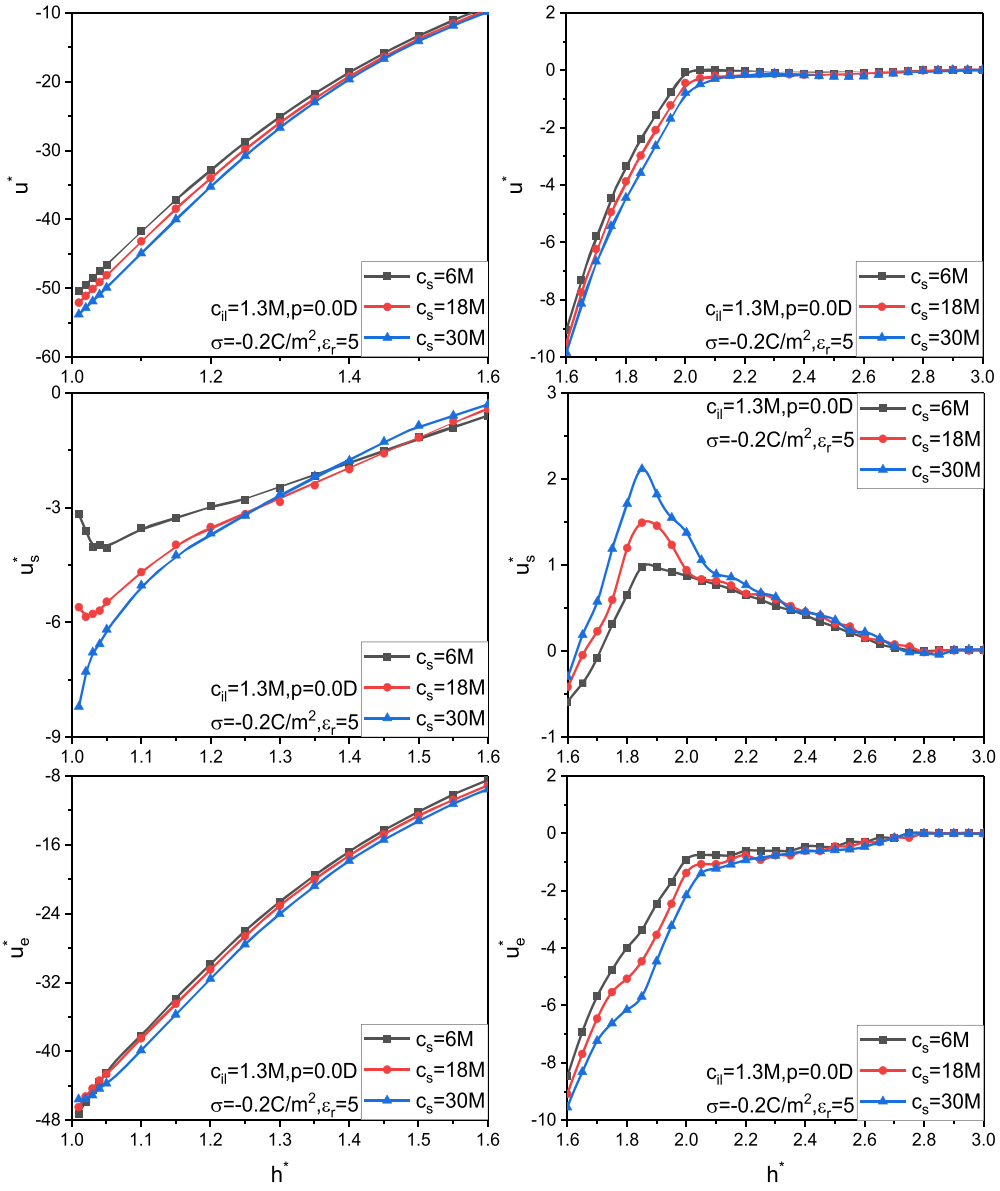


**Figure 4.** The potential energy curves (top subgraph) and its decoupled entropy term curves (middle subgraph) and energy term curves (bottom subgraph). Three solvent bulk densities are considered, they are $c_s = 6\text{M}, 18\text{M},$ and 30M,respectively. The solvent dipole moment $p = 0.0\text{D}$. System temperature of 308.15 K is considered, and other parameter values are indicated in the graphs and in the text.

(cations, anions, and positive and negative sites of solvent molecules) near the surface as a function of solvent dipole moment.

It is demonstrated that the solvent adsorption curve, when portrayed as a function of solvent dipole moment, is influenced by the size of the solution relative dielectric constant $\varepsilon_r$. In scenarios with smaller $\varepsilon_r$-values, the curve displays a maximum value. As the $\varepsilon_r$ increases, the dipole moment associated with the maximum value also becomes

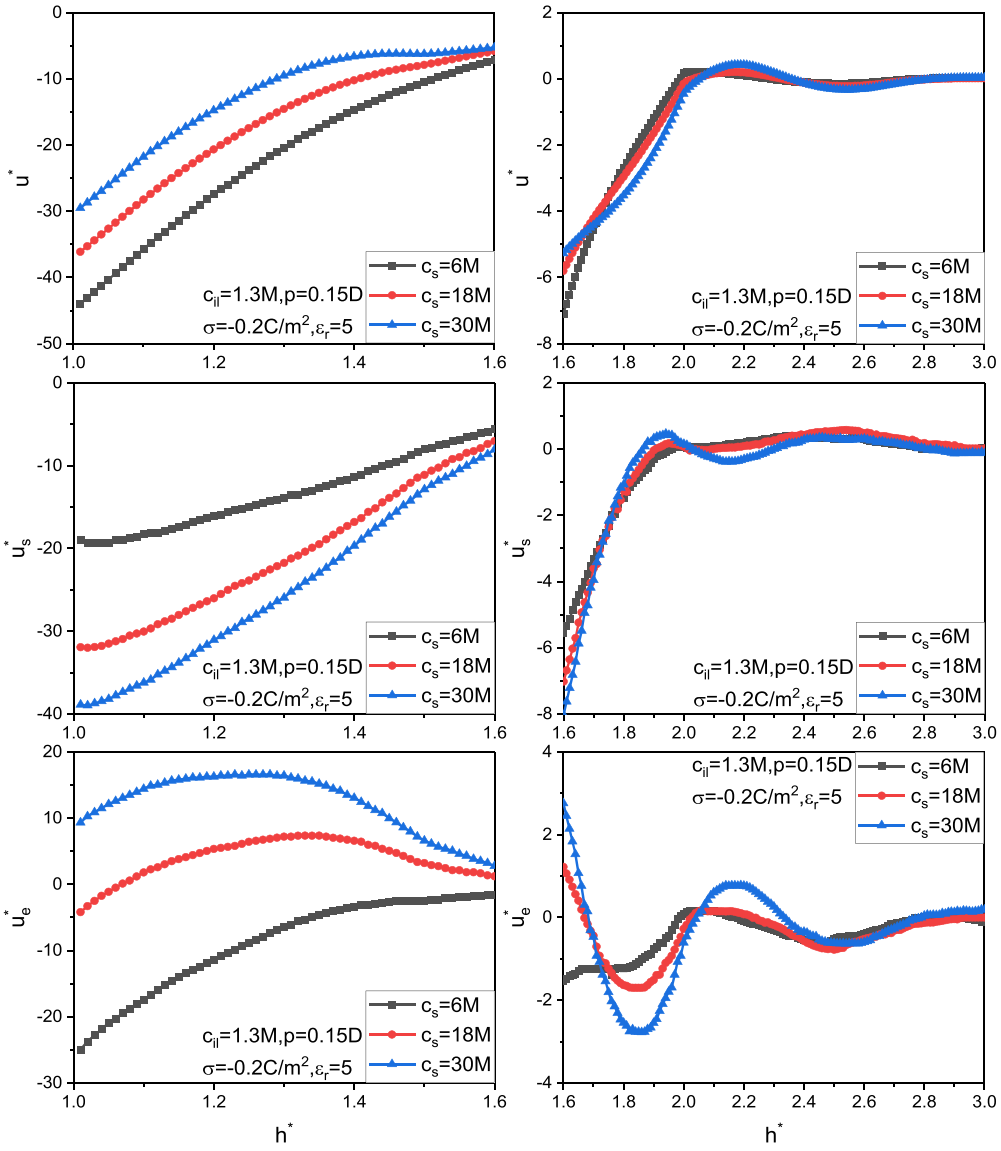


**Figure 5.** The same as in figure 4 except $p = 0.15$D.

larger. When the $\varepsilon_r$ becomes sufficiently large, the maximum value might no longer be present. An observation from figure 8 reveals that for the maximum value to disappear, the $\varepsilon_r$ may need to be greater than 20. This is because, when the dielectric constant is at 20, there is still a faint maximum value occurring at $p = 2.65$D. The above observation can be explained as follows: When the $\varepsilon_r$ is small, electrostatic interactions are stronger. The strong electrostatic interactions result in a larger adsorption of solvent and increased pore congestion. Therefore, as the dipole moment increases further, the increased electrostatic repulsion between like-charges caused by spatial crowding and raised polarized charge strength leads to a decrease in solvent adsorption with increasing dipole moments. However, even if the $\varepsilon_r$ is small, if the dipole moment is also very small, the electrostatic attraction interaction promoting solvent adsorption will not be strong.

https://doi.org/10.1088/1742-5468/ad363e


J. Stat. Mech. (2024) 043202

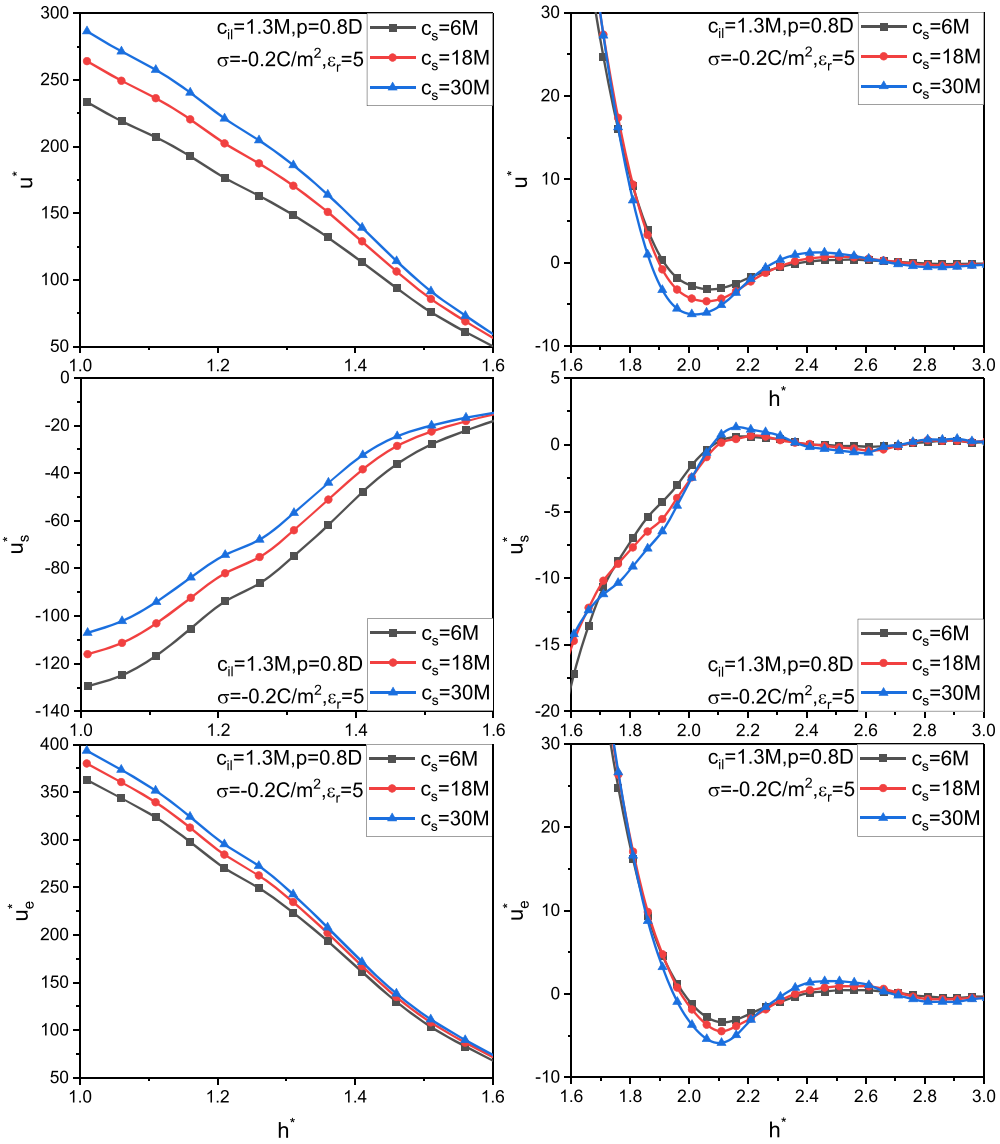


**Figure 6.** The same as in figure 4 except $p = 0.8$D.

As a result, the solvent adsorption will not be so large as to cause severe congestion inside the pore, and making it difficult for adsorption to further increase. Consequently, the adsorption is positively correlated with the dipole moment in the small dipole moment range. In contrast, if the solution $\varepsilon_r$ is large, the adsorption of solvent is naturally small, and confinement in the pore is not severe in the small dipole moment range. Only in the large dipole moment range does congestion reach a level sufficient to exhibit a maximum adsorption value. Furthermore, severe congestion might not appear in certain scenarios, allowing for solvent adsorption to increase with increasing dipole moments within a reasonably large dipole moment range. One piece of evidence supporting the above analysis is the observation that although in most dipole moment ranges, the adsorption curve with a larger $\varepsilon_r$ is below the one with a smaller $\varepsilon_r$, in the very small range of dipole

J. Stat. Mech. (2024) 043202

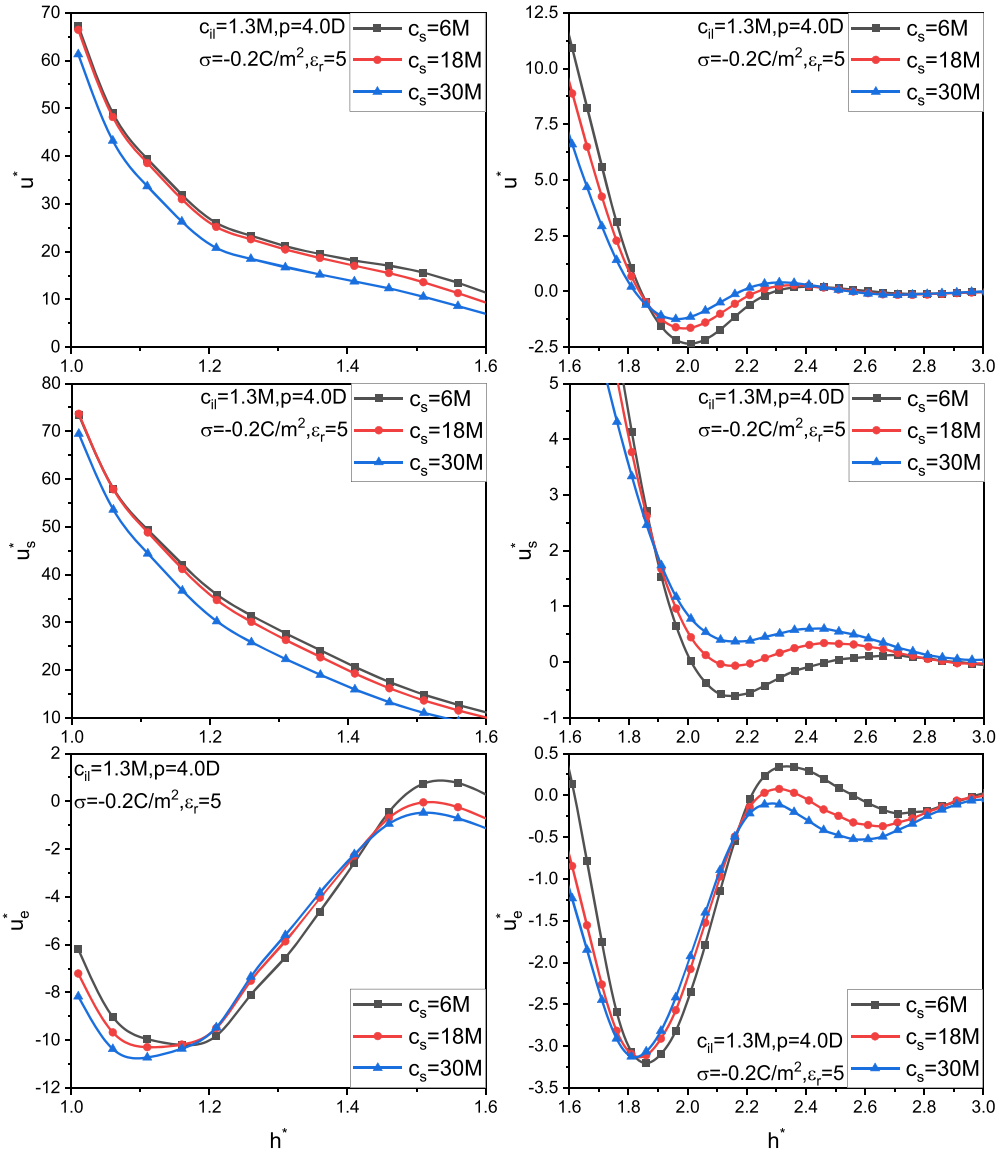


**Figure 7.** The same as in figure 4 except $p = 4.0$D.

moment approaching zero, the adsorption curve with a larger $\varepsilon_r$ is above the one with a smaller $\varepsilon_r$. According to the above analysis, this is because when the dipole moment is very small, the change in the $\varepsilon_r$ value almost does not directly affect the adsorption of the dipoles, but the reduction in electrostatic attraction caused by the increase in the $\varepsilon_r$ can significantly decrease the adsorption of counter-ions. The resulting available space indirectly increases the adsorption of the solvent. In the bulk, the dipoles form an orderly network, which is a low entropy state. Solvent adsorption disrupts this state, leading to an increase in system entropy. The larger the dipole moment, the smaller the solution dielectric constant, the more pronounced the above effect, and the more insignificant the increase in system entropy as the solvent adsorption decreases with the dipole moment. Figures 9 and 10 show that solvent in the pore exhibits a noticeable

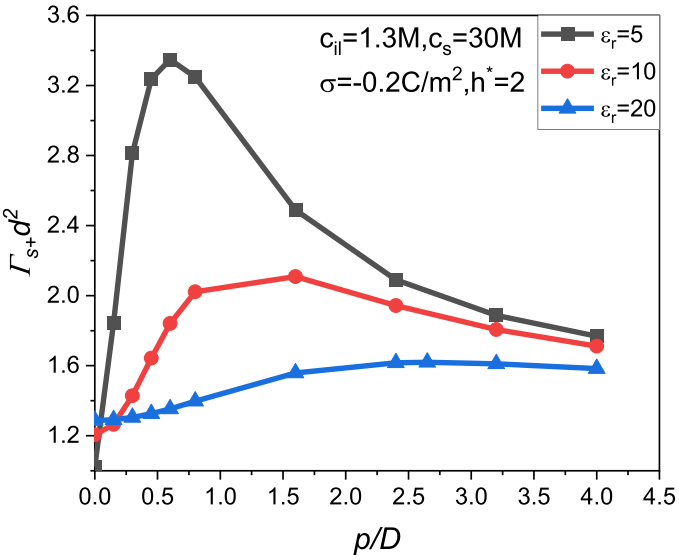


**Figure 8.** The solvent adsorption curve as a function of solvent dipole moment. Different curves correspond to different values of the relative dielectric constant of the solution. The vertical axis represents the adsorbed solvent positive site number per unit area, while the horizontal axis represents the solvent dipole moment. Values of other parameters are indicated in the graph and in the text.

stratified distribution. Specifically, the density peaks for positive and negative sites of the solvent are located at $z/d = 0.24$ and 0.72, respectively, and the difference between these two peak positions exactly equals the distance between the positive and negative sites in the solvent molecule, indicating that solvent molecules in the pore are mostly arranged perpendicular to the surface along the axis of the solvent molecule. However, thermal motion of the molecules means that this vertical arrangement is not absolute, as evidenced by the non-negligible density distribution in the middle region between these two peak positions. Furthermore, as figure 9 shows, the stratification of solvent molecules within the pore weakens with increasing solvent dipole moment. This can be inferred from the fact that the difference between the high-density peaks and the low-density valleys for both positive and negative sites of the solvent molecules decreases as the dipole moment increases. This phenomenon can be analyzed and understood through the density distribution of counterions. Figure 9 shows that as solvent adsorption decreases with increasing dipole moment, counterion adsorption generally increases, with the counterion adsorption peak located at $z/d = 0.5$, halfway between the adsorption peaks of the solvent's positive and negative sites. It is the electrostatic attraction of the counterion adsorption peak to the solvent's negative site peak that causes the solvent configuration to deviate from the absolute vertical arrangement. Clearly, the larger the dipole moment, the stronger the electrostatic attraction between the counterion adsorption peak and the solvent's negative site peak, and the greater the deviation. On the contrary, if the solution $\varepsilon_r$ reaches 20 or larger as shown in figure 8, then the solvent adsorption and stratification of solvent molecules within the pore with the change of dipole moment become completely opposite to those in figure 9, as shown in figure 10.



J. Stat. Mech. (2024) 043202

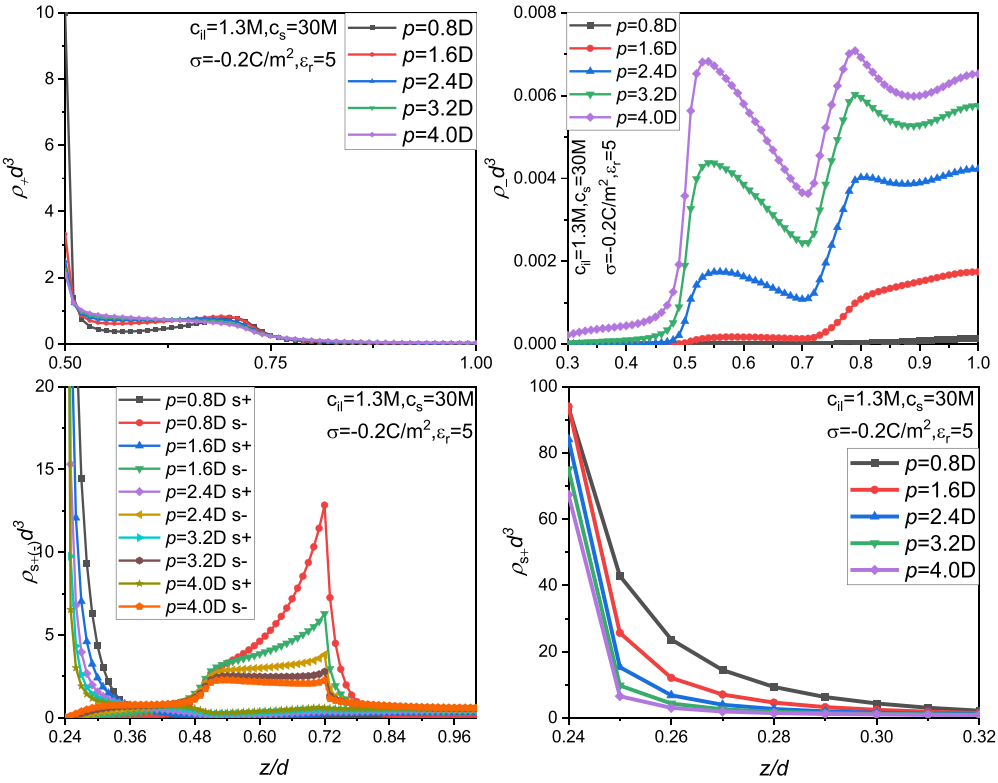


**Figure 9.** The density distribution curves for cation, anion, and positive and negative sites of solvent molecules are presented. In the two top subplots and the bottom-left subplot, curves are only drawn for the left half of the space calculated, while the other half can be deduced by symmetry. The bottom-right subplot is an enlarged view of the density distribution curves for the positive and negative sites of solvent molecules, focusing on the narrow region very close to the left charged surface. Different curves represent different values of the relative dielectric constant of the solution, and the values of other parameters are indicated in the graphs and in the text.

Although the deviation from the vertical arrangement is an entropy-increasing process, it may not be dominant compared to the entropy-reducing effect of decreased solvent adsorption as the dipole moment increases in the case of high dipole moments. Therefore, in the case of low dielectric constant in this study, the overall effect of increasing solvent dipole moments from 0.8 to 4 leads to a decrease in system entropy. As a consequence, the entropic term increases. This effect becomes more pronounced as the bulk concentration of the solvent increases. This phenomenon is already depicted in middle right subgraph of figure 7, demonstrating that as the $c_s-$value increases, the entropic term near the vicinity of the LCA minimum becomes more positive. However, around the LCA location, the energy term does not change significantly with the $c_s-$value. This is because, as the $c_s-$value increases, solvent adsorption also increases, leading to greater congestion and a subsequent increase in free energy due to particle hard-core repulsion. On the other hand, the increase in adsorption also results in enhanced electrostatic

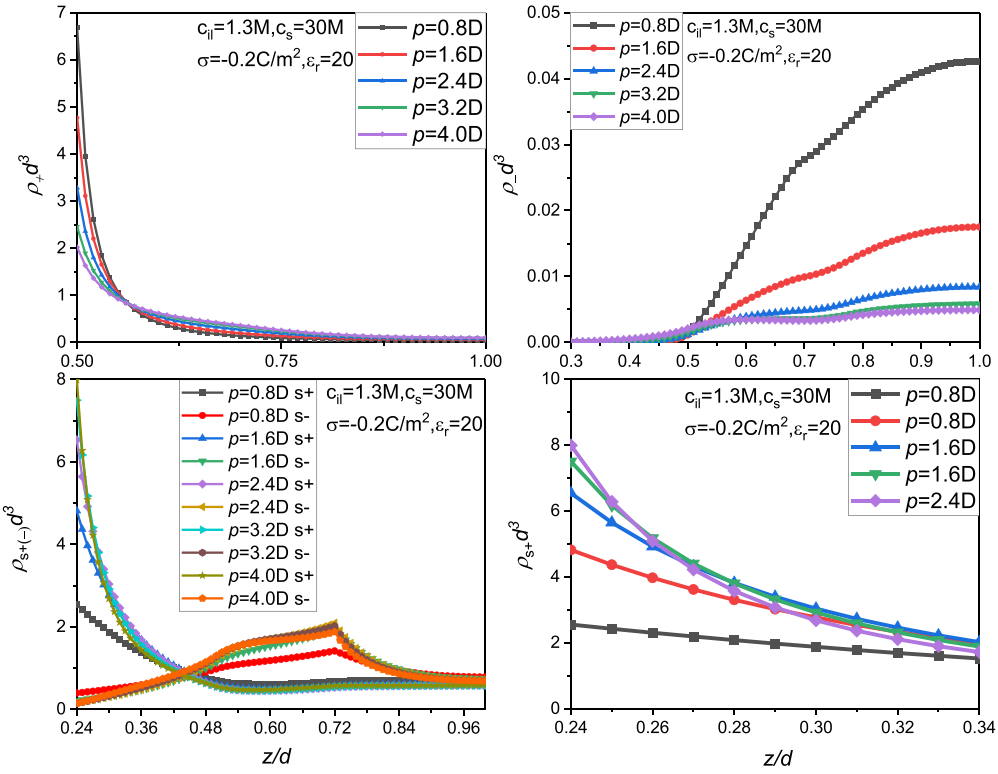


**Figure 10.** Identical to figure 9, except for different relative dielectric constants of the solution, as marked in the figure.

attraction between the walls, ions, and solvent molecules. The balance between these two changes causes the energy term to remain essentially constant with respect to the $c_s-$value, as shown in the bottom subgraph of figure 7. By considering these factors, we explain the inverse correlation between the LCA depth and the $c_s-$value for highly polar solvents. From the analysis of the solvent adsorption-dipole moment relationship mentioned above, we can understand the significant positive energy term in the case of $p = 0.8$D shown in figure 6 and the negative energy term for $p = 4.0$D shown in figure 7. In the case of $p = 0.8$D, the solvent adsorption is substantial, which increases the spatial resistance effect, leading to a rise in the free energy. In contrast, in the case of $p = 4.0$D, the decrease in solvent adsorption alleviates the spatial congestion; at the same time, the reduced pore congestion makes it easier for the positive and negative charges in the pore to adopt a conformation where the electrostatic attraction is more likely than electrostatic repulsion, and this effect is further intensified by the increase in the dipole moment. In this manner, both the intrapore congestion and electrostatic attraction factors work in the same direction, making the energy term more negative in the $p = 4.0$D scenario.

When the solvent dipole moment is relatively small, for instance, $p = 0.8$D, the solvent adsorption is considerable, as shown in figure 8, and overall, the congestion level within the pore is higher, resulting in a decrease in the system entropy. Conversely, migration from the bulk to the pore disrupts the network structure caused by dipoles

in the bulk, an effect that contributes to an increase in entropy. Overall, the entropy increase associated with solvent migration into the pores dominates the entropy loss caused by congestion within the pores. Therefore, in this case, solvent adsorption can also lead to elevated entropy, resulting in a relatively small negative entropy term around the LCA location, as depicted in figure 6. However, due to the increase of congestion, the change in the entropy term with the $c_s-$value is no longer significant, as demonstrated in figure 6. This is because, in highly congested situation, even if the bulk solvent concentration increases, it does not considerably impact the solvent adsorption. On the other hand, the increase in solvent adsorption results in a rise in particle hard-core repulsion free energy, and consequently, the energy term naturally becomes a very large positive value. Furthermore, it increases only slightly with the rise in bulk concentration, as shown in the bottom-left plot of figure 6. It should be noted that this phenomenon occurs only in the near-surface region, as the solvent positive site peak is located in this area. In the region outside the solvent positive site peak, the particle densities significantly decrease, leading to the electrostatic attraction energy between walls, ions, and dipoles dominating over the free energy caused by the hard-core repulsion. In this manner, the energy term becomes negative outside of the solvent positive site peak, and the increasing adsorption with the $c_s-$value renders the energy term more negative, as illustrated in the right-side bottom subgraph of figure 6. This explanation provides insights into the positive correlation between the LCA depth and the $c_s-$value for lower solvent polarities.

Now let us proceed to explain why the depth of LCA exhibits a non monotonic behavior with the solvent dipole moment, as shown in figure 3.

As the dipole moment decreases, for instance, from $p=4.0$D to $p=0.8$D, pore congestion increases, similar to the analysis for figure 8, and although the resulting entropy decrease becomes more significant, the entropy term is primarily influenced by the entropy increase caused by the disruption of the bulk dipole grid driven by the solvent adsorption. As a result, the entropy term assumes a negative value around the LCA location, as shown in the middle right subgraph of figure 6. On the other hand, the congestion occurs only in the near-surface region at the solvent positive site density peak, and there is no severe congestion outside of this region. In these areas, the electrostatic attraction between walls, ions, and dipoles dominates due to the increase in solvent adsorption, thereby making the energy term more negative. This effect can be observed by comparing the energy terms around the LCA location in the two bottom subgraphs in figures 6 and 7. In this manner, the LCA strength naturally becomes stronger with a decrease in the solvent dipole moment, resulting in a LCA strength maximum appearing around $p=0.5$D, as demonstrated in the middle right subgraph of figure 3.

As the dipole moment further decreases, for example, to below $p$=0.6D, say $p$ =0.15D, according to figure 8, solvent adsorption declines. As a result, the entropy increase caused by the breakdown of the bulk dipole grid accompanying the solvent adsorption is less significant; on the contrary, the entropy reduction resulting from solvent adsorption-induced congestion also becomes less substantial around the LCA location, though it still exists. Since the first factor plays a dominant role, their combination results in a more positive or less negative entropic term around the LCA location compared to the larger dipole moment case. This outcome can also be observed by

comparing the entropy terms around the LCA location in the middle right subgraphs of figures 5 and 6. To be specific, at $h^*$=1.8 (near the reduced inter-plate separation where the LCA occurs for $p = 0.15$D), the entropy term $u_s^*$ in figure 5 are around −1.0; while at $h^*$=2.0 (approaching the reduced plate spacing at which the LCA for the $p = 0.8$D case occurs), the entropy term $u_s^*$ in figure 6 are around −2.0.

On the other hand, both a reduction in solvent adsorption capacity and a decline in dipole moment result in a decreased total electrostatic attraction strength between wall-charges, dipoles, and ions, which consequently leads to an increase in the energy term. Quantitatively speaking, as depicted in the bottom right subgraphs of figures 5 and 6, for $p = 0.15$D, the energy terms at $h^* = 1.8$ are around −1.2, −1.6 and −2.5, for $c_s = 6$M, 18 M, 30 M, respectively; while for $p = 0.8$D, the energy terms at $h^* = 2.0$ are around −1.2, −1.9 and −3.7, for $c_s = 6$M, 18 M, 30 M, respectively. We interestingly note that, at two higher $c_s-$values: 18 M and 30 M, the dipole moments of $p = 0.15$D and $p = 0.8$D indeed cause significant differences in the energy terms at their respective LCA minima. However, for the smallest $c_s-$value studied, there is essentially no difference in the energy terms between the $p = 0.15$D and $p = 0.8$D scenarios. This can be understood because the magnitude of the dipole moment's effect naturally depends on the number of molecules carrying this dipole moment. As $c_s-$value becomes smaller, this effect is less likely to be evident, especially in complex systems where numerous factors also influence the magnitude of the energy term. It should be pointed out that if we compare the energy terms of the $p = 0.15$D and $p = 0.8$D scenarios uniformly at $h^* = 2.0$, we can observe the following: for $p = 0.15$D, the energy terms at $h^* = 2.0$ are around 0.093, −0.27, and −0.61, for $c_s$ =6 M, 18 M, and 30 M, respectively. As a result, the differences in the energy terms caused by $p = 0.15$D and $p = 0.8$D scenarios change more in the direction predicted by our analysis, which can be considered as a piece of corroborating evidence for the reliability of the aforementioned analysis. In summary, the overall effect is that the LCA weakens when the dipole moment is very small. In this way, we explain the positive correlation between the LCA strength and solvent dipole moment on the low solvent polarity side, as displayed in the middle right subgraph of figure 3.

Now we will discuss the variation of the NCP with solvent dipole moment.

As explained above, the variation patterns of the NCPs with the dipole moment can be categorized into several types. Firstly, when the dipole moment is very small, for instance, $p = 0.0$D, the NCP is negative, and its absolute value increases with solvent bulk concentration, which represents a typical characteristic of the AO depletion potential. Secondly, as the dipole moment slightly increases, for example from $p = 0.0$D to $p = 0.15$D, the absolute value of the negative NCPs tends to decrease; this is clearly visible in the top subgraphs of figures 3–5, and top and middle subgraphs of figure 1. The most notable observation is that the absolute value of the NCP in the $p = 0.15$D case (middle subgraph of figure 1 and top subgraph of figure 5) decreases with the solvent bulk concentration, in stark contrast to the $p = 0.0$D situation, as illustrated in the top subgraph of figure 1 and the top subgraph of figure 4. Thirdly, as the solvent dipole moment increases further, for instance, up to $p = 0.8$D, the NCP becomes positive. From figure 3, it is evident that in the regime ($p \geqslant 0.8$D), the NCP strength as a function of the solvent dipole moment exhibits a maximum value, approximately occurring around



J. Stat. Mech. (2024) 043202

$p = 1.0$D. However, in this regime, the relationship between the NCP strength and the solvent bulk concentration can be divided into three types: as the solvent dipole moment increases, the relationship transitions from a positive correlation to a weak correlation, and finally to an inverse correlation. To be specific, when the solvent dipole moment increases up to $p = 2.1$D, the NCP becomes insensitive to the solvent bulk concentration. Finally, when the dipole moment further increases, the NCP decreases with the solvent bulk concentration, but the correlation remains insignificant.

The above NCP change behavior can be explained by comprehensively considering the hard sphere repulsion free energy caused by pore congestion, electrostatic attraction, and the entropic change resulting from solvent molecules migrating from bulk into pore.

Compared to the case of a neutral solvent (figure 4), for $p = 0.15$D (figure 5), the migration of solvent molecules into the pore disrupts the network structure of the bulk, leading to an increase in system entropy. Correspondingly, the entropy term becomes more negative, which is clearly reflected in the middle left subgraph of figure 5. Moreover, figure 5 also shows that the absolute value of the entropy term clearly increases with the solvent bulk concentration. This latter characteristic is evidently due to the fact that, on one hand, solvent adsorption is still not large enough at $p = 0.15$D, as shown in figure 8. In this case, an increase in solvent bulk concentration can significantly enhance solvent adsorption, thereby increasing the entropy change and consequently, making the absolute value of the entropy term larger; on the other hand, an increase in the solvent bulk concentration strengthens the bulk dipole grid, resulting in a decrease in bulk entropy and an increase in the entropic change accompanying solvent migration into the pore. Finally, as the solvent dipole moment increases from $p = 0.0$D to $p = 0.15$D, the resultant increase in solvent adsorption inside the pore (as shown in figure 8) raises the hard-core repulsion free energy and the energy term. Moreover, this effect is obviously positively correlated with the bulk solvent concentration, as just analyzed. As a result, the near contact energy term should be less negative or positive compared with the $p = 0.0$D case, and increases with the solvent bulk concentration, as demonstrated in the bottom left subgraph of figure 5.

Figure 6 displays the potential energy curves and their decoupled results when the dipole moment is $p = 0.8$D. Compared to the case of $p = 0.15$D, figure 8 shows that $p = 0.8$D corresponds to a larger adsorption. As a result, the negative entropy term associated with the increase in entropy, and the less negative or positive energy term related to the hard sphere repulsion accompanying the solvent adsorption, as depicted in the left and middle/bottom subgraphs of figure 5, become more pronounced at $p = 0.8$D. This can be observed by comparing the middle and bottom left subgraphs in figures 5 and 6. This comparison indicates that for $p = 0.8$D, both the attractive entropy term and the positive energy term indeed become significantly larger than when $p = 0.15$D. An interesting distinction between these two dipole moment cases ($p = 0.8$D and $p = 0.15$D) is that, at $p = 0.8$D, both the entropy and energy terms exhibit smaller relative changes with solvent bulk concentration compared to those at $p = 0.15$D. This is because, as shown in figure 8, the solvent adsorption at $p = 0.8$D is significantly higher than that at $p = 0.15$D. In more congested pore, the increase in adsorption driving force due to the solvent bulk concentration becomes more limited in its effectiveness to enhance the solvent adsorption. Therefore, its impact on the entropy and energy terms is also

J. Stat. Mech. (2024) 043202

constrained, resulting in a more stable behavior of the entropy and energy terms when the solvent bulk concentration changes.

One might wonder, does not the increase in solvent adsorption also increase the electrostatic attraction energy, in addition to increasing the hard sphere repulsion free energy? Why does the energy term necessarily become more positive? This is because, in the $p = 0.8$D scenario, solvent adsorption is very large, and the hard sphere repulsion free energy as a function of density is quite steep at high densities. As a result, the increase in free energy due to hard sphere repulsion dominates over the decrease in free energy caused by electrostatic attraction. Consequently, the energy term is much larger than at $p = 0.15$D, leading to not only a positive total NCP but also a positive correlation between the total NCP and solvent bulk concentration, as illustrated in the top subgraph of figure 6 and the bottom subgraph of figure 1.

As the solvent dipole moment further increases, for example, from $p = 0.8$D to $p = 4.0$D, the solvent adsorption decreases, as shown in figure 8. Correspondingly, the entropy increase associated with the migration of solvent from the bulk into the pore becomes less significant. Although at the same time, the alleviation of intrapore congestion leads to an increase in entropy, the decrease in entropy increase due to reduced solvent adsorption plays a more dominant role. Therefore, overall the entropy increase at $p = 4.0$D is smaller than that at $p = 0.8$D. In this way, the entropy term changes from negative at $p = 0.8$D to positive or less negative at $p = 4.0$D, as illustrated in the middle subgraph of figure 7. Simultaneously, the decrease in solvent adsorption leads to a reduction in free energy due to hard sphere repulsion, while the electrostatic attraction becomes stronger due to the increase in dipole moment. Thus, the electrostatic attraction in the pore eventually dominates the hard sphere repulsion, causing the energy term to change from a large positive value in the case of small dipole moments, such as $p = 0.8$D, to a small negative value in the case of high dipole moments, such as $p = 4.0$D, as shown in the bottom subgraph of figure 7.

Figures 4–7 illustrate the potential energy curves and their decoupled terms, the entropy term and the energy term, at $T = 308.15$ K, for dipole moments $p = 0.0$D, $p = 0.15$D, $p = 0.8$D, and $p = 4.0$D, respectively. Coincidentally, figures 1 and 2 also depict the potential energy curves for these dipole moment values but at $T = 298.15$ K. By comparing these corresponding curves, we can obtain the impact of temperature on the potential energy curves of our system. Since molecular thermal motion is ubiquitous, the influence of potential energy curves on the system's thermodynamic properties is always determined by the relative values of potential energy versus thermal motion energy. Therefore, to analyze differing temperature potential energy curves, we should compare the relative values of potential energy and thermal motion energy, making it appropriate to compare the reduced potential energy curves at different temperatures.

Upon comparison, we find that, at these two temperatures, the potential energy curves exhibit similar shapes and qualitatively display similar variations with respect to system parameters. However, there are quantifiable differences that can be observed even though both temperatures fall within the normal range for biological systems. More specifically, one finds that regardless of whether the potential energy at the contact point is positive or negative, the reduced potential strength is always higher at lower temperatures compared to higher temperatures. Similarly, for the well depth of the LCA,

J. Stat. Mech. (2024) 043202

the well is slightly deeper at lower temperatures. This temperature effect has notable macroscopic implications, which can substantially impact the behavior and properties of systems at larger scales. The LCA well depth determines the stability of molecular arrangements and the binding of biomolecules with their ligands, whereas the contact potential strength is related to the formation (or absence) of particle pairs. Furthermore, contact potential strength influences the formation of gels, networks, or aggregates, as well as mechanical properties such as elasticity, viscosity, and deformation.

There have been some research reports on the interplay of electrostatic interactions and entropic effect. It is concluded [66–68] through theory and experiment that when binary colloidal species are moderately charged, the electrostatic repulsion force between large and small colloids will enhance the exclusion of the small particles from the larger ones. This effect enhances at low ionic strength the depletion attraction even for very low concentration of small colloidal component. In literature [69] an electrostatic-enhanced depletion attraction is observed by adding charged nonadsorbing polymers to electrostatically structured suspensions of charged liposomes; in particular, it is shown that the depletion attraction is especially long ranged, and is dominated by electrostatic effects rather than entropic ones. Again, it is considered that electrostatic-enhanced depletion attraction arises from the fact that the charged polymers are removed away from the region around the liposomes, as a consequence of the electrostatic repulsion between the liposome and charged polymer.

The above studies [66–69] have all emphasized the direct relationship between the depletion potential and adsorption of small particles or polyelectrolyte chains near the similarly charged large colloidal particle. In our system, the primary depletant is an overall neutral dimer short chain with a certain dipole moment, and its bulk concentration is generally higher than that of the depletants reported in the literature [66–69]. The differences between our system and other ones [66–69] led us to observe a far richer set of phenomena. In real systems, the relationship between entropy change and depletant adsorption is more complex, and their impact on the EIP is subject to electrostatic interactions between charged particles or dimer sites and surface charges, as well as spatial hindrance effects, and their coupling.

Unlike in the AO model, where the entropy change related to depletant adsorption simply originates from the increase in the system's entropy due to the expansion of particle free mobility space in the bulk caused by the overlap of repulsion layers around each large particle, in our more realistic system, it also depends on whether the three-dimensional grid formed by the solvent molecules' electrical dipoles in the bulk is destroyed due to their adsorption, which can also lead to an entropy increase. Additionally, the increase/decrease in solvent adsorption caused by the dipole moment change can result in congestion/congestion alleviation within the pore, which is also a factor contributing to the decrease/increase in system entropy. Consequently, in more realistic systems, whether the adsorption of depletant at the surface of large-size particle leads to an increase or decrease in system entropy depends on the relative magnitudes of these three factors. The interesting non-monotonic variations of the entropy term in the EIP with respect to system parameters that we observed in the figures are a combined reflection of the impacts of these three factors on the entropy change. Furthermore, the adsorption of dimer solvent molecules with dipoles causes two effects regarding the

J. Stat. Mech. (2024) 043202

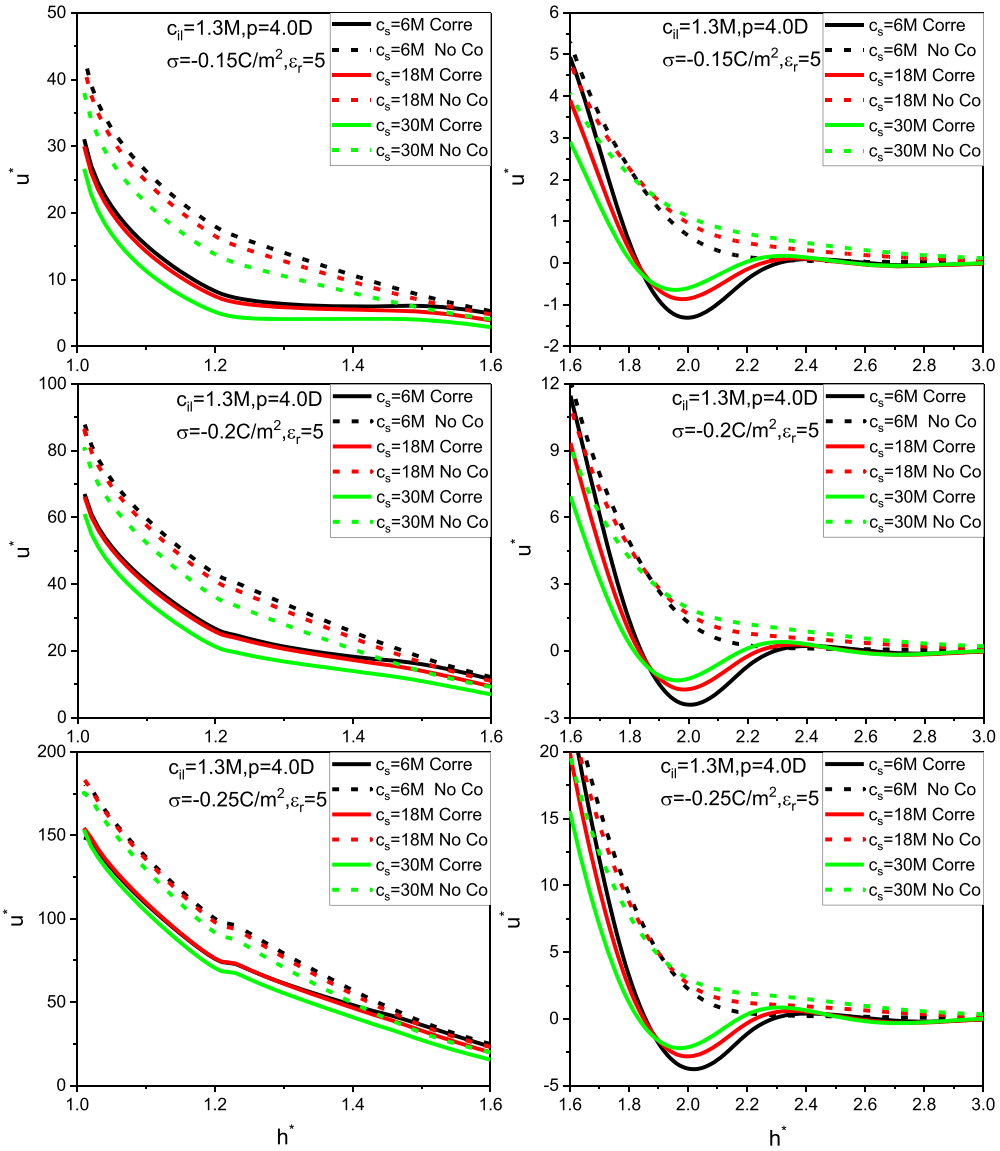


**Figure 11.** Comparison of effective interaction potential (EIP) with and without considering correlation effect. Top, middle, and bottom plots correspond to different surface charge densities, as indicated in the graphs. Values of other parameters are indicated in the graphs and in the text.

system's free energy. On one hand, the hard-core repulsion between ions, dimer sites, and the surface charges will result in an increase in the system's free energy, with the extent of this increase significantly growing as the congestion rises. On the other hand, in the presence of high-dipole-moment solvent molecules within the pore, electrostatic attraction also contributes to reducing the system free energy. This is because particles inside the pore will spontaneously adjust their relative positions in order to minimize their free energy. It is apparent that the decrease in the system's free energy caused by net electrostatic attraction is positively correlated with the solvent molecules' dipole

moment. The former effect contributes to inducing a positive energy term in the EIP, while the latter effect contributes to a negative energy term.

Figure 11 illustrates the impact of the electrostatic correlation on the EIP by examining the difference between considering and disregarding the correlation effect between the hard sphere repulsion and electrostatic interactions, which can simply be done by retaining or removing the $F_{coup}[\{\rho_i\}]$ term from equation (2). We can observe that the correlation effect exerts a qualitative impact on EIP: it is precisely the correlation effect that results in the emergence of LCA in 1:1 electrolyte solutions. Nevertheless, numerous past theoretical and simulation studies [70, 71] have demonstrated that in the absence of dipolar solvent, solely relying on correlation effect is insufficient to produce the LCA in the presence of mono-valent counterions only, under typical conditions (when the values of electrolyte bulk concentration and surface charge density are not exceedingly large). This suggests that the presence of dipolar solvent can facilitate the emergence of LCA.

In summary, it is precisely due to the diversity of factors that affect the system's entropy change and their interplay with the electrostatic, hard-core interactions, as well as the coupling effect between electrostatic and hard-core interactions, that give rise to more diverse and interesting EIP curve shapes in the current system than before. This provides new methods and corresponding molecular mechanisms for regulating the EIP in complex systems.

## 4. Summary

We investigated the influences of solvent polarity and solvent bulk concentration on the EIP between similarly charged surfaces in the simultaneous presence of IL and dimer solvent. Through the dimer dipole model, we considered the solvent molecule's non-spherical structure and polarity; by the cDFT functionals, we comprehensively considered the hard sphere repulsion, electrostatic interactions, and their coupling in our analysis. Consequently, the cDFT calculations in this article take into account the comprehensive and synergistic effects arising from various inter-particle interactions and entropy effects caused by depletant adsorption on the EIP. This approach provides a more accurate and holistic understanding of the phenomena involved in more realistic systems.

Several non monotonic EIP behaviors are found. Firstly, the LCA strength at plate separation approximately equal to sum of the counter-ion diameter and the solvent molecule length exhibits non-monotonicity with the solvent dipole moment. Secondly, in different solvent dipole moment intervals, depth of the LCA monotonically increases, decreases, or remains almost constant with the solvent bulk concentration. Thirdly, the NCP varies non-monotonically with the solvent dipole moment, which can be attractive for very small dipole moments and repulsive for high polarities. Finally, the NCP exhibits five different patterns as the solvent bulk concentration changes. In the very low solvent polarity regime, the NCP is attractive, its strength increases (neutral solvent) and decreases ($p = 0.15$D) with the solvent bulk concentration. In the case of non very weakly polar solvents, the repulsive NCP always occur; in this regime, as the solvent polarity increases, the NCP strength is positively correlated with (such as $p = 0.8$D),

insensitive to (such as $p = 2.15$D), and weakly and negatively correlated with (such as $p = 4.0$D) the solvent bulk concentration.

By decoupling the EIP into entropy and energy terms, we found that the interesting phenomena disclosed in this work originate from the synergistic change of these two terms with system parameters; the cause of their respective changes lies in the non-monotonic variation of solvent adsorption with the solvent molecule dipole moment. Particularly, it is found that the entropy change accompanying the solvent migration into the pore depends on multiple factors, such as pore congestion and the destruction of the dipole grid in the bulk, in addition to the overlap of exclusion layers surrounding each large particle surface, which is the primary mechanism previously disclosed by means of the AO model. The use of the more sophisticated dimer dipole model and cDFT method reveals the interplay of various factors that contribute to a more nuanced understanding of the system.

From the above analysis, we can clearly see that the electrostatic interaction, originating from the charged surface and the polarized charges carried by the polar solvent molecule, has a significant correction effect on the entropy term caused by the oversimplified AO model, endowing the total EIP with a more diverse morphology. The current theoretical analysis also provides more diverse means for regulation of the EIP, allowing scientists to model complex systems more tractably and gain insights into the fundamental behaviors of matter at the microscopic scale. This, in turn, helps in developing efficient and reliable nano devices for various applications in fields such as electronics, sensors, and nanotechnology.

## Acknowledgments

We sincerely appreciate the invaluable comments and suggestions provided by the reviewers, which have led to a more in-depth and comprehensive discussion in our paper. This project is supported by the National Natural Science Foundation of China (Grants 22173117). This work is supported in part by the High Performance Computing Center of Central South University.

## References

[1] Neefjes I, Halonen R, Vehkamaki H and Reischl B 2022 Modeling approaches for atmospheric ion-dipole collisions: all-atom trajectory simulations and central field methods *Atmos. Chem. Phys.* **22** 11155–72
[2] Pandey P K and Chandra A 2023 Mechanism, kinetics, and potential of mean force of evaporation of water from aqueous sodium chloride solutions of varying concentrations *J. Phys. Chem.* B **127** 4602–12
[3] Tagliaro I, Di Credico B and Moncho-Jordá A 2020 Electrostatic depletion effects on the stability of colloidal dispersions of sepiolite and natural rubber latex *J. Colloid Interface Sci.* **560** 606–17
[4] Afsaneh H and Elliott J A W 2022 Charge-dipole attraction as a surface interaction between water droplets immersed in organic phases *Langmuir* **38** 13121–38
[5] Zhu H J, Whittle A J and Pellenq R J M 2022 Potential of mean force for face-face interactions between pairs of 2:1 clay mineral platelets *Langmuir* **38** 13065–74
[6] Palaia I, Goyal A, Del Gado E, Samaj L and Trizac E 2022 Like-charge attraction at the nanoscale: ground-state correlations and water destructuring *J. Phys. Chem.* B **126** 3143–9
[7] Martinez-Leon A and Hub J S 2023 Overcoming hysteresis in ligand binding potential of mean force calculations *Biophys. J.* **122** 143A

[8] Soto-Bustamante F, Valadez-Pérez N E, Liu Y, Castañeda-Priego R and Laurati M 2022 Clusters in colloidal dispersions with a short-range depletion attraction: thermodynamic identification and morphology *J. Colloid Interface Sci.* **618** 442–50
[9] Wan Y E, Wang X, Chou I-M and Li X 2021 Role of sulfate in the transport and enrichment of REE in hydrothermal systems *Earth Planet. Sci. Lett.* **569** 117068
[10] Guan Q, Mei Y, Etschmann B, Testemale D, Louvel M and Brugger J 2020 Yttrium complexation and hydration in chloride-rich hydrothermal fluids: a combined ab initio molecular dynamics and in situ x-ray absorption spectroscopy study *Geochim. Cosmochim. Acta* **281** 168–89
[11] Shvets A A and Semenov A N 2013 Effective interactions between solid particles mediated by free polymer in solution *J. Chem. Phys.* **139** 054905
[12] de Los Santos-lopez N M, Perez-Angel G, Mendez-Alcaraz J M and Castaneda-Priego R 2021 Competing interactions in the depletion forces of ternary colloidal mixtures *J. Chem. Phys.* **155** 024901
[13] Mustakim M and Kumar A V A 2022 Depletion induced demixing and crystallization in binary colloids subjected to an external potential barrier *J. Phys. Chem.* B **126** 327–35
[14] Zhou X M, Lei L J, Zeng Y Q, Lu X, Liang F, Zhang L and Lin G 2023 High salinity effects on the depletion attraction in colloid-polymer mixtures *J. Colloid Interface Sci.* **631** 155–64
[15] Chaimovich A and Shell M S 2013 Length-scale crossover of the hydrophobic interaction in a coarse-grained water model *Phys. Rev.* E **88** 052313
[16] Naito H, Okamoto R, Sumi T and Koga K 2022 Osmotic second virial coefficients for hydrophobic interactions as a function of solute size *J. Chem. Phys.* **156** 221104
[17] Engstler J and Giovambattista N 2022 Different temperature- and pressure-effects on the water-mediated interactions between hydrophobic, hydrophilic, and hydrophobic-hydrophilic nanoscale surfaces *J. Chem. Phys.* **157** 064701
[18] Dal Molin J P and Caliri A 2018 Entropic formulation for the protein folding process: hydrophobic stability correlates with folding rates *Physica* A **490** 1111–24
[19] Klos J S and Paturej J 2022 Binding mechanisms in dendrimer-surfactant complexes *Phys. Rev.* E **105** 034501
[20] Jaiswal S, He Y F and Lu H P 2022 Probing functional conformation-state fluctuation dynamics in recognition binding between calmodulin and target peptide *J. Chem. Phys.* **156** 055102
[21] Vedadghavami A, He T F, Zhang C Z, Amiji S M, Hakim B and Bajpayee A G 2022 Charge-based drug delivery to cartilage: hydrophobic and not electrostatic interactions are the dominant cause of competitive binding of cationic carriers in synovial fluid *Acta Biomater.* **151** 278–89
[22] Kage S, Imamura K and Ishida N 2023 Evaluation of interaction forces between hydrophobic surfaces in surfactant solutions by atomic force microscopy *Colloid Polym. Sci.* **301** 775–82
[23] Majee A, Bier M and Dietrich S 2016 Poisson-Boltzmann study of the effective electrostatic interaction between colloids at an electrolyte interface *J. Chem. Phys.* **145** 064707
[24] Yigit C, Heyda J and Dzubiella J 2015 Charged patchy particle models in explicit salt: ion distributions, electrostatic potentials, and effective interactions *J. Chem. Phys.* **143** 064904
[25] Bakhshandeh A, Dos Santos A P, Diehl A and Levin Y 2015 Interaction between random heterogeneously charged surfaces in an electrolyte solution *J. Chem. Phys.* **142** 194707
[26] Bakhshandeh A, Dos Santos A P and Levin Y 2020 Interaction between charge-regulated metal nanoparticles in an electrolyte solution *J. Phys. Chem.* B **124** 11762–70
[27] Zhou S 2020 Inter-surface effective electrostatic interactions in the presence of surface charge discreteness and solvent granularity *Mol. Phys.* **118** e1778807
[28] Budkov Y A and Kolesnikov A L 2022 Modified Poisson-Boltzmann equations and macroscopic forces in inhomogeneous ionic fluids *J. Stat. Mech.* **2022** 053205
[29] Filippov A V and Starov V M 2023 Electrostatic and van der Waals interactions of nanoparticles in electrolytes *JETP Lett.* **117** 598–605
[30] Zhou S 2023 Effective electrostatic interaction between columnar colloids: roles of solvent steric hindrance, polarity, and surface geometric characteristics *Mol. Phys.* **121** e2216632
[31] Mimura M, Tsumura K, Matsuda A, Akatsuka N and Shiraki K 2019 Effect of additives on liquid droplet of protein-polyelectrolyte complex for high-concentration formulations *J. Chem. Phys.* **150** 064903
[32] Cheng W J and McClements D J 2016 Biopolymer-stabilized conjugated linoleic acid (CLA) oil-in-water emulsions: impact of electrostatic interactions on formation and stability of pectin-caseinate-coated lipid droplets *Colloids Surf.* A **511** 172–9
[33] Hate S S, Reutzel-Edens S M and Taylor L S 2020 Influence of drug-silica electrostatic interactions on drug release from mesoporous silica-based oral delivery systems *Mol. Pharm.* **17** 3435–46

J. Stat. Mech. (2024) 043202

[34] Mauri E, Chincarini G M F, Rigamonti R, Magagnin L, Sacchetti A and Rossi F 2017 Modulation of electrostatic interactions to improve controlled drug delivery from nanogels *Mater. Sci. Eng.* C **72** 308–15
[35] Malysheva O, Tang T and Schiavone P 2008 Adhesion between a charged particle in an electrolyte solution and a charged substrate: electrostatic and van der Waals interactions *J. Colloid Interface Sci.* **327** 251–60
[36] Bordag M, Klimchitskaya G L, Mohideen U and Mostepanenko V M 2009 *Advances in the Casimir Effect* (*International Series of Monographs on Physics*) vol 145 (OUP, Oxford)
[37] Napiórkowski M and Pruszczyk M 2022 Variance of the Casimir force in an ideal Bose gas *J. Stat. Mech.* **2022** 073104
[38] Dzyaloshinskii I E, Lifshitz E M and Pitaevskii L P 1961 General theory of van der Waals forces *Adv. Phys.* **10** 165
[39] Karimipour I, Kanani A, Koochi A, Keivani M and Abadyan M 2015 Modeling the electromechanical behavior and instability threshold of NEMS bridge in electrolyte considering the size dependency and dispersion forces *Physica* E **74** 140–50
[40] Guo H Y, Stan G and Liu Y 2018 Nanoparticle separation based on size-dependent aggregation of nanoparticles due to the critical Casimir effect *Soft Matter* **14** 1311–8
[41] Faruk M M and Biswas S 2018 Repulsive Casimir force in Bose-Einstein condensate *J. Stat. Mech.* **ID** 043401
[42] Squarcini A, Romero-Enrique J M and Parry A O 2023 Derivation of the Casimir contribution to the binding potential for 3D wetting *Mol. Phys.* **121** e2193654
[43] Sahu R and Nayar D 2021 Crowding effects on water-mediated hydrophobic interactions *J. Chem. Phys.* **155** 024903
[44] Bogunia M, Liwo A, Czaplewski C, Makowska J, Giełdoń A and Makowski M 2022 Influence of temperature and salt concentration on the hydrophobic interactions of adamantane and hexane *J. Phys. Chem.* B **126** 634–42
[45] Bogunia M and Makowski M 2020 Influence of ionic strength on hydrophobic interactions in water: dependence on solute size and shape *J. Phys. Chem.* B **124** 10326–36
[46] Ge L X, Shi X, Li B Z and Gong K 2023 Fluctuation-induced dispersion forces on thin DNA films *Phys. Rev.* E **107** 064402
[47] Zhou S 2020 On the statistical mechanics investigation of structure and effective electrostatic force between two solid surfaces in electrolyte dissolved in non-polar solvent *J. Stat. Mech.* **2020** 073210
[48] Zhou S 2022 Effective electrostatic forces between two neutral surfaces with surface charge separation: valence asymmetry and dielectric constant heterogeneity *Mol. Phys.* **120** e2094296
[49] Zhou S and Bakhshandeh A 2023 Interaction between two overall neutral charged microscopically patterned surfaces *J. Chem. Phys.* **159** 044706
[50] Zhou S 2023 On capacitance enhancement at decreasing pore width and its relation with solvent concentration and polarity *J. Electrochem. Soc.* **170** 090536
[51] Jain S, Dominik A and Chapman W G 2007 Modified interfacial statistical associating fluid theory: a perturbation density functional theory for inhomogeneous complex fluids *J. Chem. Phys.* **127** 244904
[52] Rosenfeld Y 1989 Free-energy model for the inhomogeneous hard-sphere fluid mixture and density-functional theory of freezing *Phys. Rev. Lett.* **63** 980
[53] Percus J K 1976 Equilibrium state of a classical fluid of hard rods in an external field *J. Stat. Phys.* **15** 505–11
[54] Vanderlick T K, Davis H T and Percus J K 1989 The statistical mechanics of inhomogeneous hard rod mixtures *J. Chem. Phys.* **91** 7136–45
[55] Reiss H, Frisch H L and Lebowitz J L 1959 Statistical mechanics of rigid spheres *J. Chem. Phys.* **31** 369–80
[56] Lutsko J F 2020 Explicitly stable fundamental-measure-theory models for classical density functional theory *Phys. Rev.* E **102** 062137
[57] Rosenfeld Y, Schmidt M, Löwen H and Tarazona P 1997 Fundamental-measure free-energy density functional for hard spheres: dimensional crossover and freezing *Phys. Rev.* E **55** 4245
[58] Roth R, Evans R, Lang A and Kahl G 2002 Fundamental measure theory for hard-sphere mixtures revisited: the White Bear version *J. Phys.: Condens. Matter* **14** 12063–78
[59] Mansoori G A, Carnahan N F, Starling K E and Leland T W Jr 1971 Equilibrium thermodynamic properties of the mixture of hard spheres *J. Chem. Phys.* **54** 1523–5
[60] Blum L 1975 On the localized pay-off model and its application to double layer theory *Mol. Phys.* **30** 1529–36
[61] Hiroike K 1977 New approach to the double layer of colloidal and biological models including electrical double layers *Mol. Phys.* **33** 1195–203
[62] Lebowitz J L 1964 Exact solution of the Percus–Yevick equation for a mixture of hard spheres *Phys. Rev.* **133** A895–9
[63] Zhou S and Lamperski S 2022 Unusual properties of the electric double layer in an extremely narrow nanotube. A grand canonical Monte Carlo and classical DFT study *J. Phys. Chem. Solids* **161** 110440

J. Stat. Mech. (2024) 043202

[64] Zhou S, Lamperski S and Zydorczak M 2014 Properties of a planar electric double layer under extreme conditions investigated by classical density functional theory and Monte Carlo simulations *J. Chem. Phys.* **141** 064701
[65] Zhou S, Lamperski S and Sokołowska M 2017 Classical density functional theory and Monte Carlo simulation study of electric double layer in the vicinity of a cylindrical electrode *J. Stat. Mech.* **2017** 073207
[66] Buzzaccaro S, Piazza R, Colombo J and Parola A 2010 Enhancement of depletion forces by electrostatic depletant repulsion *J. Chem. Phys.* **132** 124902
[67] Peláez-Fernández M, Moncho-Jordá A and Callejas-Fernández J 2011 Charged colloid-polymer mixtures: a study on electrostatic depletion attraction *J. Chem. Phys.* **134** 054905
[68] Ojeda-Mendoza G J, Moncho-Jordá A, González-Mozuelos P, Haro-Pérez C and Rojas-Ochoa L F 2018 Evidence of electrostatic-enhanced depletion attraction in the structural properties and phase behavior of binary charged colloidal suspensions *Soft Matter* **14** 1355–64
[69] Peláez-Fernández M, Moncho-Jordá A, García-Jimeno S, Estelrich J and Callejas-Fernández J 2012 Role of the electrostatic depletion attraction on the structure of charged liposome-polymer mixtures *Phys. Rev.* E **85** 051405
[70] Poon W C K and Andelman D (ed) 2006 *Soft Condensed Matter Physics in Molecular and Cell Biology* (CRC Press/Taylor & Francis)
[71] Israelachvili J N 2011 *Intermolecular and Surface Forces* 3rd edn (Academic)

J. Stat. Mech. (2024) 043202